

# NeuroNAS: A Framework for Energy-Efficient Neuromorphic Compute-in-Memory Systems using Hardware-Aware Spiking Neural Architecture Search

Rachmad Vidya Wicaksana Putra, Muhammad Shafique

*eBrain Lab, New York University (NYU) Abu Dhabi, Abu Dhabi, United Arab Emirates*

{rachmad.putra, muhammad.shafique}@nyu.edu

**Abstract**—Spiking Neural Networks (SNNs) have demonstrated capabilities for solving diverse machine learning tasks with ultra-low power/energy consumption. To maximize the performance and efficiency of SNN inference, the Compute-in-Memory (CIM) hardware accelerators with emerging device technologies (e.g., RRAM) have been employed. However, SNN architectures are typically developed without considering constraints from the application and the underlying CIM hardware, thereby hindering SNNs from reaching their full potential in accuracy and efficiency. To address this, we propose *NeuroNAS*, a novel framework for developing energy-efficient neuromorphic CIM systems using a hardware-aware spiking neural architecture search (NAS), i.e., by quickly finding an SNN architecture that offers high accuracy under the given constraints (e.g., memory, area, latency, and energy consumption). *NeuroNAS* employs the following key steps: (1) optimizing SNN operations to enable efficient NAS, (2) employing quantization to minimize the memory footprint, (3) developing an SNN architecture that facilitates an effective learning, and (4) devising a systematic hardware-aware search algorithm to meet the constraints. Compared to the state-of-the-art, *NeuroNAS* with 8bit weight precision quickly finds SNNs that maintain high accuracy by up to 6.6x search time speed-ups, while achieving up to 92% area savings, 1.2x latency speed-ups, 84% energy savings across CIFAR-10, CIFAR-100, and TinyImageNet-200 datasets; while the state-of-the-art fail to meet all constraints at once. In this manner, *NeuroNAS* enables efficient design automation in developing energy-efficient neuromorphic CIM systems for diverse ML-based applications.

**Index Terms**—Spiking neural networks (SNNs), neuromorphic computing, compute-in-memory (CIM), neural architecture search (NAS)

## I. INTRODUCTION

In recent years, neuromorphic computing has shown remarkable performance of spiking neural networks (SNNs) in solving diverse machine learning (ML) tasks with ultra-low-power/energy consumption. To maximize SNNs’ algorithmic performance and efficiency gains, many studies have been conducted, ranging from the developments of SNN models [1]–[3], hardware accelerators [4]–[6], as well as their deployments for diverse applications, such as image classification [7] [8], object recognition in automobile [9] [10], continual learning in autonomous systems [11]–[14], embodied intelligence in robotics [15], and bio-signal processing in healthcare [16]. To maximize the efficiency of SNN processing, SNN hardware accelerators have been employed. However, they still suffer from high memory access energy that dominates the overall system energy (i.e., *the memory wall bottleneck*); see Fig. 1(a). To address this, the non-von Neumann Compute-in-Memory (CIM) paradigm with non-volatile memory (NVM) technologies, such as resistive random access memory (RRAM), has been investigated [17] [18]. Specifically, CIM platforms minimize data movements between the memory and compute engine parts, hence the memory access energy.

However, simply executing the existing SNNs on a CIM platform may not fulfill the design requirements from the application (e.g., accuracy and latency) and hardware constraints (e.g., memory, area, and energy consumption), as SNN models are typically developed without considering the characteristics of the CIM hardware. Moreover, most of SNN models are derived from conventional Artificial Neural Networks (ANNs), whose operations are different from SNNs, thus they may lose unique SNN features (e.g., temporal information) that leads to sub-optimal accuracy [2]. This limitation is also observed

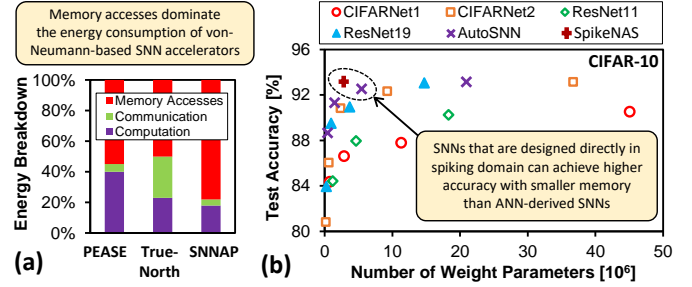


Fig. 1. (a) Energy breakdown of SNN inference on von-Neumann-based neuromorphic accelerators: PEASE [19], TrueNorth [4], and SNNAP [20]; adapted from [21]. (b) Accuracy vs. memory of different SNNs on CIFAR-10: CIFARNet1 [22], CIFARNet2 [23], ResNet11 [24], ResNet19 [25], AutoSNN [1], and SpikeNAS [3]; adapted from studies in [1] [3].

in recent studies [2] [3], i.e., designing SNNs in the spiking domain can achieve higher accuracy than deriving from the ANN domain; see Fig. 1(b). Furthermore, different ML-based applications have different requirements of algorithmic performance and efficiency. Therefore, to ensure the practicality of SNNs for real-world implementations, SNN developments have to meet the design requirements and constraints. In fact, *maximizing SNN benefits for the targeted applications and CIM platforms requires SNN developments that can meet the expected performance, efficiency, and constraints*, which is a non-trivial task. Moreover, manually developing the suitable SNN is time consuming and laborious, hence requiring an alternative technique that can find a desired solution efficiently.

**Research Problem:** *How to automatically and quickly develop an SNN architecture for neuromorphic CIM systems that achieves high accuracy and efficiency (for latency and energy consumption) under the given memory and area constraints?* An efficient solution to this problem may enable automatic and quick developments of energy-efficient neuromorphic CIM systems for diverse ML applications.

### A. State-of-the-Art and Their Limitations

Currently, state-of-the-art works focus on employing *neural architecture search (NAS)* for finding SNN architectures that achieve high accuracy [1]–[3] [26]–[30]. However, *all of these NAS methods do not consider multiple design requirements and constraints posed by the target application and the CIM hardware (i.e., memory, area, latency, and energy consumption)*, thereby limiting the applicability of neuromorphic CIM systems for diverse real-world applications. To illustrate the limitations of state-of-the-art and the optimization potentials, a case study is performed and discussed in Sec. I-B.

### B. Case Study and Associated Research Challenges

We study the impact of applying constraints in NAS process. Here, we reproduce the state-of-the-art NAS for SNNs (i.e., SNASNet [2]), and then apply a memory constraint of  $2 \times 10^6$  (2M) parameters on it to build a memory-aware SNASNet, while considering the CIFAR-100 dataset. For the processing hardware, we consider an RRAM-based CIM hardware platform from [18]. Note, the details of experimental

setup are discussed in Sec. IV. The experimental results are shown in Fig. 2, from which we make the following key observations.

- A smaller SNN may achieve comparable accuracy to the bigger one, showing possibility to obtain high accuracy with low memory.
- Memory saving leads to the reduction of area, latency, and energy consumption of SNN processing on a CIM platform.

From these observations, we identify **associated research challenges** to be addressed for solving the research problem below.

- The solution should consider multiple design requirements and constraints (i.e., memory, area, latency, and energy consumption) in its search algorithm to ensure the deployability of SNNs for the target application and the CIM platform.
- The solution should quickly perform its searching process to minimize the searching time.

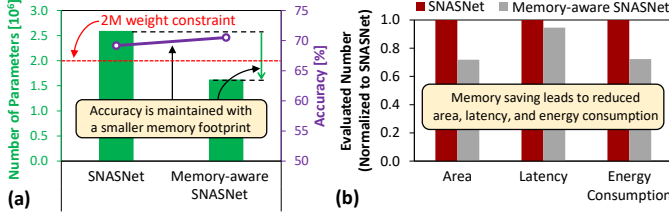


Fig. 2. Experimental results of the case study considering the CIFAR-100: (a) number of weight parameters and accuracy; and (b) area, latency, and energy consumption when running networks on an RRAM-based CIM platform [18].

### C. Our Novel Contributions

To address the research challenges, we propose **NeuroNAS**, a *novel framework for quickly finding the SNN architecture that can achieve high accuracy, while meeting the application requirements and CIM constraints (i.e., memory, area, latency, and energy consumption) through hardware-aware spiking NAS*. It is also the first work that develops an integrated hardware-aware spiking NAS for developing energy-efficient neuromorphic CIM systems. NeuroNAS employs the following key steps (see an overview in Fig. 3 and details in Fig. 5).

- 1) **Optimization of SNN Operations:** It aims to investigate and selects SNN operations that have positive impact on accuracy, while considering their memory costs. The selected operations are used for building a network architecture.
- 2) **Development of Network Architectures:** It aims to build a network that facilitates effective learning and efficient deployments on CIM. It leverages (1) the selection of SNN operations, and (2) the quantization-aware fitness evaluation policy to improve the quality of fitness function and optimize the network size.
- 3) **A Hardware-aware Search Algorithm:** It aims to find a network architecture that achieves high accuracy by searching for suitable neural architectures, while considering the given memory, area, latency, and energy constraints.

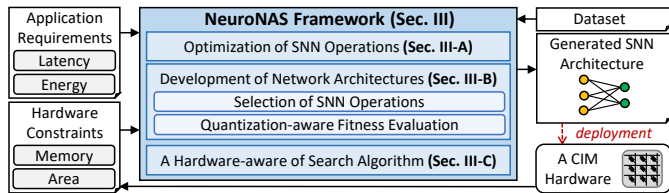


Fig. 3. Overview of our novel contributions in the NeuroNAS framework.

**Key Results:** We evaluate NeuroNAS framework through a PyTorch implementation, and run it on Nvidia RTX A6000 GPU machines. Experimental results show that, NeuroNAS with 8bit weight precision quickly finds SNNs that maintain high accuracy by up to 6.6x search time speed-ups, while achieving up to 92% area savings, 1.2x latency speed-ups, 84% energy savings across

CIFAR-10, CIFAR-100, and TinyImageNet-200 datasets compared to the state-of-the-art. Meanwhile, the state-of-the-art fail to meet all constraints at once.

## II. PRELIMINARIES

### A. NAS for SNNs

**Overview:** The focus of state-of-the-art works is still on the NAS development for finding SNN architectures that achieve high accuracy. These works can be categorized into two approaches. First, *NAS with Training* approach, which aims to train a super-network that contains all possible architecture candidates, and then search a subset of architecture that meets the fitness criteria; as shown in [1] [27]. However, it incurs huge searching time, memory, and energy consumption. Second, *NAS without Training* approach, which overcomes the limitations of “*NAS with Training*” by directly evaluating the fitness scores of architecture candidates, then only training the one with the highest score [2] [3] [26] [28]–[30]. However, *all these state-of-the-art methods do not consider multiple design requirements and constraints posed by the target application and the CIM platform*, hence limiting their applicability for diverse real-world applications.

**NAS without Training:** In this work, we consider the “*NAS without training*” approach due to its efficiency in finding an appropriate network without costly training. This concept was initially proposed for ANNs [31], then adopted in spiking domain. For instance, SNASNet [2] leverages the studies in [31] for evaluating the investigated SNN based on their representation capabilities, which indicate their potentials in learning effectively. It employs the following key steps.

- 1) It feeds mini-batch samples ( $S$ ) to the network, then records the LIF neurons’ activities. If  $U_m$  reaches  $\theta$ , the corresponding neuron is mapped to 1, and otherwise 0. In each layer, this mapping is represented as binary vector ( $b$ ).
- 2) The Hamming distance  $H(b_i, b_j)$  between samples  $i$  and  $j$  is calculated to construct a matrix ( $\mathbf{M}_H$ ); see Eq. 1.  $N$  is the number of neurons in the investigated layer, while  $\beta$  is the normalization factor to address high sparsity issue from LIF neurons.
- 3) Afterward, the fitness score ( $F$ ) of each investigated architecture candidate is calculated using  $F = \log(\det |\sum_l \mathbf{M}_H^l|)$ , and the one with highest-score is selected for training.

$$\mathbf{M}_H = \begin{pmatrix} N - \beta H(b_1, b_1) & \cdots & N - \beta H(b_1, b_S) \\ \vdots & \ddots & \vdots \\ N - \beta H(b_S, b_1) & \cdots & N - \beta H(b_S, b_S) \end{pmatrix} \quad (1)$$

In this work, we propose a similar approach but enhanced with *quantization-aware mechanism in our NeuroNAS framework to adapt to the CIM configuration*, which will be discussed in Sec. III-B2.

**Neural Cell-based Strategy for NAS:** It aims to provide a unified benchmark for NAS algorithms [32]. A *neural cell* (or simply *cell*) is a directed acyclic graph (DAG), that is originally designed with 4 nodes and 5 pre-defined operations, and its 2 nodes are connected to each other via a specific pre-defined operation [2] [32]; see Fig. 4. Its idea is to search for the cell architecture and operations. In this work, we employ a similar neural cell-based strategy in our NeuroNAS framework but optimized for enabling a quick search and high accuracy, which will be discussed in Sec. III-A - Sec. III-B1.

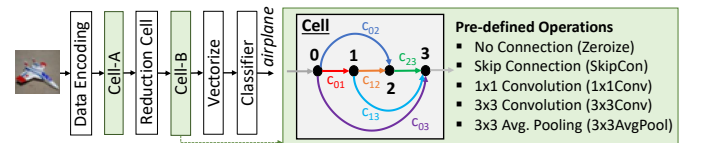


Fig. 4. The SNN macro-architecture with 2 neural cells, and each cell is a DAG whose edge denotes a specific pre-defined operation; adapted from [2].

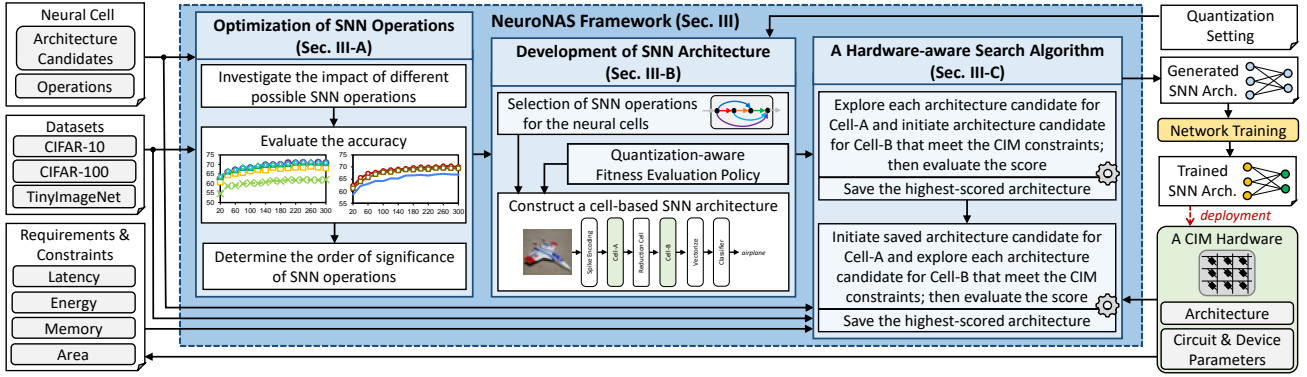


Fig. 5. Overview of our NeuroNAS framework, and its key steps for generating an SNN architecture that can achieve high accuracy while meeting the given memory, area, latency, and energy constraints; the novel contributions are highlighted in blue.

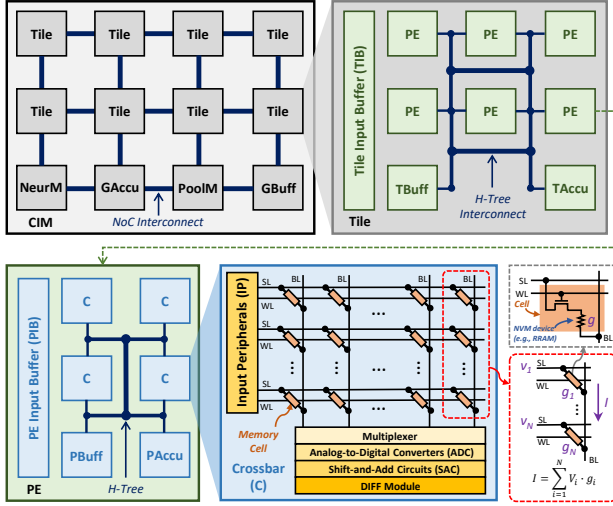


Fig. 6. The CIM hardware architecture that is considered in this work. It is based on the SpikeFlow architecture [18].

### B. CIM Hardware Architecture and SNN Mapping Strategy

**Architecture:** We employ the state-of-the-art CIM hardware for SNNs (i.e., SpikeFlow [18]), whose architecture is presented in Fig. 6. It comprises compute tiles (Tiles), a neuron module (NeurM), a global accumulator (GAccu), a pooling module (PoolM), and a global buffer (GBuf). These modules are connected to each other using network-on-chip (NoC) connection. Each tile comprises a tile input buffer (TIB), processing elements (PEs), a tile buffer (TBuf), and a tile accumulator (TAccu). Each PE comprises a PE input buffer (PIB), a number of crossbars (C), PE buffer (PBuf), and PE accumulator (PAccu). These modules are connected to each other using H-Tree connection. Meanwhile, each crossbar comprises input peripherals (IP), an array of NVM devices, multiplexers, analog-to-digital converter (ADC), shift-and-add circuit (SAC), and DIFF module to perform signed multiply-and-accumulate (MAC) operations.

**SNN Mapping:** We employ the state-of-the-art mapping strategy on the CIM hardware in SpikeSim [18]; see Fig. 7. Its idea is to distribute weights across the crossbars, while exploiting weights and feature maps reuse. If we consider dimensions of  $H \times H \times D$  for input feature maps (*ifms*),  $P \times P \times D \times F$  for weights (*wghs*), and  $X \times X$  for crossbar, then the mapping strategy can be described as follows.

- Weight kernel elements in  $P \times P$  are mapped on different crossbars. For instance, a  $3 \times 3$  weight kernel needs 9 crossbars; see C1-C9.
- Elements from  $1 \times 1$  weight kernel along the channel  $D$  are mapped along a column of the crossbars (i.e.,  $1 \times 1 \times D$ ); see C1<sub>1</sub> - C1<sub>9</sub>.
- Different weight filters are mapped on different columns of the same crossbar. For instance, 4 weight filters will occupy 4 columns

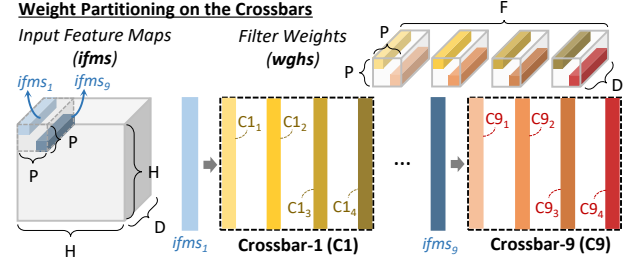


Fig. 7. SNN partitioning for mapping input feature maps (*ifms*) and weights (*wghs*) on the CIM crossbars; adapted from studies in [18]. The dimension of *ifms* is denoted as  $H \times H \times D$ , while *wghs* is denoted as  $P \times P \times D \times F$ .

in the same crossbar; see C1<sub>1</sub> - C1<sub>4</sub>.

- A similar partitioning is applied to *ifms* over the  $P \times P \times D$  block. Furthermore, this mapping strategy considers a design choice that a network layer can be mapped on multiple CIM tiles, but multiple network layers cannot be mapped in one CIM tile [18].

## III. THE NEURONAS FRAMEWORK

We propose NeuroNAS framework to address the research challenges, whose key steps are discussed below (see overview in Fig. 5).

### A. Optimization of SNN Operations

To develop an efficient SNN architecture that offers high accuracy, we have to understand the significance of its operations, then select the ones that lead to high accuracy with small memory cost. To do this, we perform an experimental case study with following scenarios.

- **Scenario-1:** We remove an operation from the pre-defined ones (i.e., Zeroize, SkipCon,  $1 \times 1$ Conv,  $3 \times 3$ Conv, and  $3 \times 3$ AvgPool one-by-one), then perform NAS to evaluate the impact of their removal.
- **Scenario-2:** We investigate the impact of other possible operations with different kernel sizes (i.e.,  $5 \times 5$ Conv and  $7 \times 7$ Conv) on accuracy and memory cost, to explore their potentials as alternative solutions. To do this, we replace the operation that has the role of extracting features from pre-define ones (i.e.,  $3 \times 3$ Conv) with the investigated operation (either  $5 \times 5$ Conv or  $7 \times 7$ Conv).

All these scenarios consider a cell-based SNN architecture shown in Fig. 4 and the CIFAR-100 workload. Experimental results are shown in Fig. 8, from which we make the following key observations.

- ① Eliminating Zeroize,  $1 \times 1$ Conv, and  $3 \times 3$ AvgPool from the search space does not significantly degrade the accuracy as compared to the baseline. Hence, these operations can be removed from the search space. If model compression is needed for reducing the memory size, we can keep  $3 \times 3$ AvgPool in the search space.
- ② Eliminating SkipCon from the search space slightly reduces accuracy, since SkipCon is useful for providing feature maps from previous layer to preserve important information. Similar

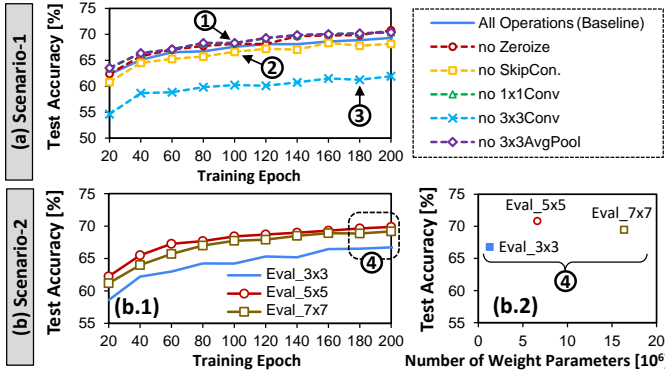


Fig. 8. (a) Results of eliminating different operations from the search space of the cell architecture. (b) Results of investigating the impact of 5x5Conv and 7x7Conv. Here, Eval\_3x3, Eval\_5x5, and Eval\_7x7 refer to then accuracy when evaluating the impact of 3x3Conv, 5x5Conv, and 7x7Conv, respectively.

results are also observed in [33]. Hence, SkipCon should be kept in the search space to maintain the learning quality.

- ③ Eliminating 3x3Conv from the search space significantly degrades accuracy, since the main role of 3x3Conv is to extract important features from input samples. Hence, 3x3Conv should be kept in the search space to maintain the learning quality.
- ④ Employing 5x5Conv and 7x7Conv can improve accuracy, since larger kernel sizes are capable of extracting more unique features from input samples. However, they incur higher memory overheads, which lead to higher latency and energy consumption.

These observations show the order of significance of the operations for achieving high accuracy with low memory cost, from the highest to the lowest: (1) 3x3Conv, (2) SkipCon, (3) 3x3AvgPool, then (4) 5x5Conv, 7x7Conv, Zeroize, and 1x1Conv. This information is then leveraged in Sec. III-B1.

### B. Development of SNN Architecture

This step aims to build an SNN architecture that facilitates effective learning. Toward this, it considers two parts: (1) development of the neural cell architecture, and (2) development of the SNN architecture.

1) **Neural Cell Architecture:** Our discussion in Sec. III-A show that we can optimize the search space of cell-based NAS strategy for maintaining/improving the accuracy while keeping the memory small. To do this, we select a few operations that have positive impact on accuracy with low memory cost to be considered in the search space. Specifically, we consider SkipCon, 3x3Conv, and 3x3AvgPool in the search space, while keeping 4 nodes of DAG in the neural cell.

2) **SNN Architecture:** The CIM platforms typically store the SNN weights in NVM devices (e.g., RRAM) using a fixed-point format due to its efficient implementation [18]. How each weight value stored in CIM hardware depends on the precision of NVM devices and SNN weights. For instance, a multi-bit weight value may be stored in several single-level-cell (SLC) devices, or in a single multi-level-cell (MLC) device. This indicates that SNNs should be developed and optimized considering the CIM parameters (e.g., NVM device precision) to ensure the deployability of SNNs. However, simply performing post-training quantization (PTQ) with fixed-point format may significantly degrade the accuracy; see ⑤ in Fig. 9(a). To address this, we propose a *Quantization-aware Fitness Evaluation (QaFE) policy* for quantizing the network candidates during NAS, thereby compressing the network size while improving the fitness function. Our QaFE policy employs the following key steps; see Fig. 9(b).

- An architecture candidate is built based on the given cell configuration (i.e., for topology and optimized operations).
- Weight quantization is then performed for the investigated network based on the precision level and the rounding scheme.

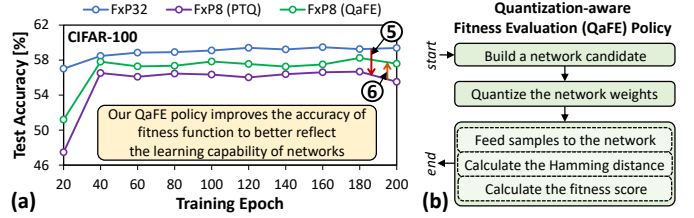


Fig. 9. (a) Results of an experimental case study considering the CIFAR-100 dataset for networks with different fixed-point precision levels: 32-bit weights (Fxp32), 8-bit weights with PTQ (Fxp8-PTQ), and 8-bit with QaFE (Fxp8-QaFE). (b) Key steps in our novel QaFE policy.

- Afterward, mini-batch samples  $S$  are fed to the network to calculate the Hamming distances between different samples, build a matrix  $M_H$ , and calculate the fitness score  $F$ .

In this manner, the fitness function is enhanced to better reflect the representation capability of the quantized network rather than the fitness score from the original network; see ⑥ in Fig. 9(a).

### C. A Hardware-aware Search Algorithm

To systematically incorporate the proposed optimizations and perform the QaFE policy in the NAS process while meeting multiple design requirements and constraints, we propose a novel hardware-aware search algorithm. Its pseudo-code is shown in Alg. 1, whose key steps are discussed below.

- Each cell has an individual search to determine its internal architecture by exploring possible candidates from different combinations of architectures from multiple cells: Cell-A and Cell-B.
- First, we explore possible architectures inside the Cell-A (Alg. 1: line 3-5). Here, the Cell-B architecture is initially set the same as Cell-A (Alg. 1: line 6). Then, we build an SNN based on Cell-A and Cell-B, and quantize it (Alg. 1: line 7-8).
- Afterward, we evaluate the SNN memory cost considering the number of SNN weight parameters (Alg. 1: line 9-10). If memory constraint is met, then we perform the fitness evaluation (Alg. 1: line 11). If the fitness score is higher than the saved one, we record the SNN architecture as a solution candidate (Alg. 1: line 12-16).
- Second, we explore possible architectures inside the Cell-B (Alg. 1: line 3 and 17-18). Then, we build an SNN based on the states of Cell-A and Cell-B, and quantize it (Alg. 1: line 19-20).
- Afterward, we evaluate the candidate for its memory, area, latency, and energy costs (Alg. 1: line 21-25). If all constraints are met, we proceed with the fitness function evaluation (Alg. 1: line 26). If the fitness score is higher than the saved one, then we record the SNN architecture as a solution candidate (Alg. 1: line 27-30).
- After all steps are finished, we consider the saved SNN architecture as the solution of NAS (Alg. 1: line 31) which is ready to train.

To enable quick and accurate area, latency, and energy calculations in the NAS, we also propose adjustments considering the precision of NVM device ( $bit_D$ ) and SNN weights ( $bit_W$ ). Specifically, we propose to employ  $\lceil bit_W / bit_D \rceil$  as an adjustment factor of the corresponding calculations for allocating the crossbar area and calculating the energy consumption, and which also affect the processing latency.

## IV. EVALUATION METHODOLOGY

To evaluate NeuroNAS framework, we build an experimental setup and tools flow as shown in Fig. 10, while considering the widely-used evaluation settings in the SNN community [34]–[37]. For design constraints, we consider 10M parameters for memory,  $1000mm^2$  for area,  $500ms$  for latency, and  $1000\mu J$  for energy budgets.

**Software Evaluation:** To evaluate our NeuroNAS framework, we develop a PyTorch implementation based on the SpikingJelly [38], then run it on the Nvidia GeForce RTX A6000 GPU machines. We

### Algorithm 1 Our Hardware-aware Search Algorithm

**INPUT:** [1] Number of cell operations ( $P$ ): SkipCon=0, 3x3Conv=1, 3x3AvgPool=2;  
[2] Design requirements and constraints: memory ( $const_{mem}$ ), area ( $const_{area}$ ), latency ( $const_{lat}$ ), energy consumption ( $const_{eng}$ );  
**OUTPUT:** Generated an SNN architecture ( $net\_arch$ );

```

BEGIN
Initialization:
1:  $score_h = -1000$ ;
Process:
2: for ( $i=0$ ;  $i < 2$ ;  $i++$ ) do
3:   for each combination from ( $\forall c_{01} \in \{0, \dots, P-1\}$ ), ( $\forall c_{02} \in \{0, \dots, P-1\}$ ),
   ( $\forall c_{03} \in \{0, \dots, P-1\}$ ), ( $\forall c_{12} \in \{0, \dots, P-1\}$ ), ( $\forall c_{13} \in \{0, \dots, P-1\}$ ),
   ( $\forall c_{23} \in \{0, \dots, P-1\}$ ) do
4:     if ( $i==0$ ) then
5:        $cell_A = cell(c_{01}, c_{02}, c_{03}, c_{12}, c_{13}, c_{23})$ ;
6:        $cell_B = cell_A$ ;
7:        $arch = net(cell_A, cell_B)$ ;
8:        $arch_q = quant(arch)$ ;
9:        $cost_{mem} = calc\_memory(arch_q)$ ;
10:      if ( $cost_{mem} \leq const_{mem}$ ) then
11:         $score = fitness\_eval(arch_q)$ ;
12:        if ( $score > score_h$ ) then
13:           $score_h = score$ ;
14:           $saved\_cell_A = cell_A$ ;
15:           $saved\_cell_B = cell_B$ ;
16:           $net\_arch = arch_q$ ;
17:        end if
18:      end if
19:    if ( $i==1$ ) then
20:       $cell_B = cell(c_{01}, c_{02}, c_{03}, c_{12}, c_{13}, c_{23})$ ;
21:       $arch = net(saved\_cell_A, cell_B)$ ;
22:       $arch_q = quant(arch)$ ;
23:       $cost_{mem} = calc\_memory(arch_q)$ ;
24:       $cost_{area} = calc\_area(arch_q)$ ;
25:       $cost_{lat} = calc\_latency(arch_q)$ ;
26:       $cost_{eng} = calc\_energy(arch_q)$ ;
27:      if ( $cost_{mem} \leq const_{mem}$ ) and
28:      ( $cost_{area} \leq const_{area}$ ) and
29:      ( $cost_{lat} \leq const_{lat}$ ) and
30:      ( $cost_{eng} \leq const_{eng}$ ) then
31:         $score = fitness\_eval(arch_q)$ ;
32:        if ( $score > score_h$ ) then
33:           $net\_arch = arch_q$ ;
34:           $score_h = score$ ;
35:           $saved\_cell_B = cell_B$ ;
36:        end if
37:      end if
38:    end for
39: end for
return  $net\_arch$ ;
END

```

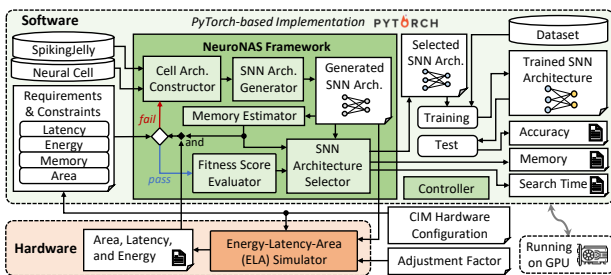


Fig. 10. The experimental setup and tools flow.

train the network using a surrogate gradient learning [39] [40] with 200 epochs. To show the generality of our solution, we consider the CIFAR-10, CIFAR-100, and TinyImageNet-200 which represent simple, medium, and complex datasets, respectively. For the comparison partner, we consider the state-of-the-art SNASNet with its default settings (e.g., 5000x random search iterations) [2]. We also assume 32bit fixed-point (FxP32) for SNASNet implementation on CIM hardware, as there is no quantization in SNASNet. Outputs of this evaluation are the accuracy, memory cost, and searching time.

**Hardware Evaluation:** To evaluate the area, latency, and energy consumption, we employ the energy-latency-area (ELA) simulator

TABLE I

THE CIM CIRCUIT AND NVM (RRAM) DEVICE PARAMETERS CONSIDERED IN THE ELA SIMULATOR; ADAPTED FROM STUDIES IN [18].

Circuit Parameters			
NoC Topology & Width	Mesh & 32bits	Size of GBuff	20KB
Clock Frequency	250MHz	Size of TBuff	10KB
Number of Crossbar-per-PE	9	Size of PBuff	5KB
Number of PE-per-Tile	8	Size of TIB	50KB
Multiplexer Size	8	Size of PIB	30KB
Precision of Crossbar ADC	4bits	$V_{DD}$	0.9V
Column Parasitic Resistance	5 $\Omega$	$V_{read}$	0.1V
RRAM Device Parameters [41]			
Bit(s)-per-Cell	1	$R_{on}$	20k $\Omega$
Write Variation	0.1	$R_{off}$	200k $\Omega$

while considering the SpikeFlow CIM hardware architecture with real measurements-based RRAM device values from the studies in [18]. The circuit and device parameters are shown in Table I.

## V. RESULTS AND DISCUSSION

### A. Maintaining High Accuracy

Fig. 11 shows the experimental results of the accuracy. The state-of-the-art SNASNet achieves 90.79%, 67.18%, and 53% accuracy for the CIFAR-10, CIFAR-100, and TinyImageNet-200, respectively. These are obtained through the network generation in SNASNet, which simply relies on the random search iteration. Meanwhile, our NeuroNAS can achieve comparable accuracy to the state-of-the-art with smaller precision levels (i.e., with at least 8bits), as shown by ❶ for CIFAR-10, ❷ for CIFAR-100, and ❸ for TinyImageNet-200. For CIFAR-10, NeuroNAS achieves accuracy of 91.44% (FxP16), 90.53% (FxP14), 88.92% (FxP12), 88.27% (FxP10), and 83.44% (FxP8). For CIFAR-100, NeuroNAS achieves accuracy of 63.90% (FxP16), 60.74% (FxP14), 59.87% (FxP12), 59.83% (FxP10), and 57.59% (FxP8). Meanwhile, for TinyImageNet-200, NeuroNAS achieves accuracy of 53% (FxP16), 53% (FxP14), 57% (FxP12), 59% (FxP10), and 53% (FxP8). These results indicate that, our NeuroNAS can still preserve the high accuracy as compared to the state-of-the-art across different datasets while employing smaller precision levels. Moreover, in the TinyImageNet-200 case, NeuroNAS can consistently achieve similar or even higher accuracy to the state-of-the-art. The reasons are the following: (1) NeuroNAS only employs cell operations that have high significance and positive impact on the accuracy, and (2) NeuroNAS constructs the network by considering its fitness score under quantized weights, hence enabling more accurate evaluation of network candidates and search toward the desired SNN architecture.

### B. Ensuring Hardware-aware SNN Generation

Fig. 12 shows the experimental results for hardware-related evaluation, i.e, memory, area, latency, and energy consumption.

**Memory:** Both SNASNet and our NeuroNAS satisfy the memory constraint. SNASNet incurs 1.28M weight parameters for CIFAR-10, and 1.93M for CIFAR-100 and TinyImageNet-200. Meanwhile, NeuroNAS incurs 888K-4.7M weight parameters for CIFAR-10, 1.77M-4.72M for CIFAR-100, and 1.77M-3.83M for TinyImageNet-200 across different precisions (i.e., FxP4-FxP16). These are obtained as NeuroNAS incorporates the memory constraint in its NAS algorithm.

**Area:** SNASNet generates networks that occupy area of 634mm<sup>2</sup> for CIFAR-10 and CIFAR-100, and 755mm<sup>2</sup> for TinyImageNet-200; see ❹. Since SNASNet does not consider the area constraint, the hardware area of the generated network is not under control during its NAS process. Moreover, in each neural cell, there are multiple convolutional (CONV) layers which cannot be mapped in the same CIM tile due to the mapping strategy. This mapping forces the CIM processing to utilize more resources (e.g., CIM tiles). Meanwhile, our NeuroNAS generates networks that occupy area of 26mm<sup>2</sup>-187mm<sup>2</sup> for CIFAR-10 (70%-96% savings from SNASNet), 25mm<sup>2</sup>-209mm<sup>2</sup>

Our NeuroNAS can maintain high accuracy for its generated quantized SNNs, hence making them comparable to SNNs without quantization from the state-of-the-art.

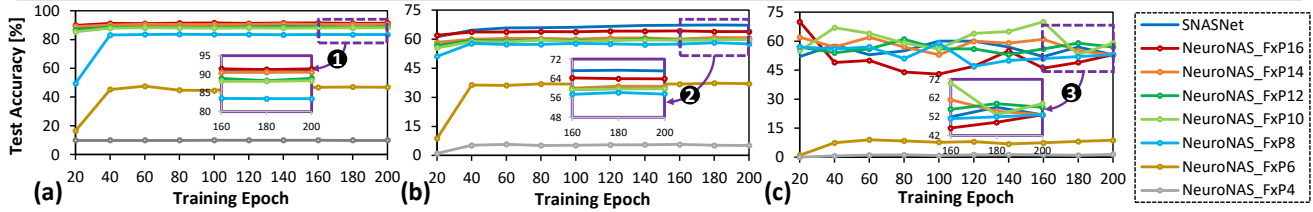


Fig. 11. Experimental results of the test accuracy achieved by the SNASNet and our NeuroNAS across training epochs and different precision levels (i.e., FxP16, FxP14, FxP12, FxP10, FxP8, FxP6, and FxP4) for (a) CIFAR-10, (b) CIFAR-100, and (c) TinyImageNet-200 workloads.

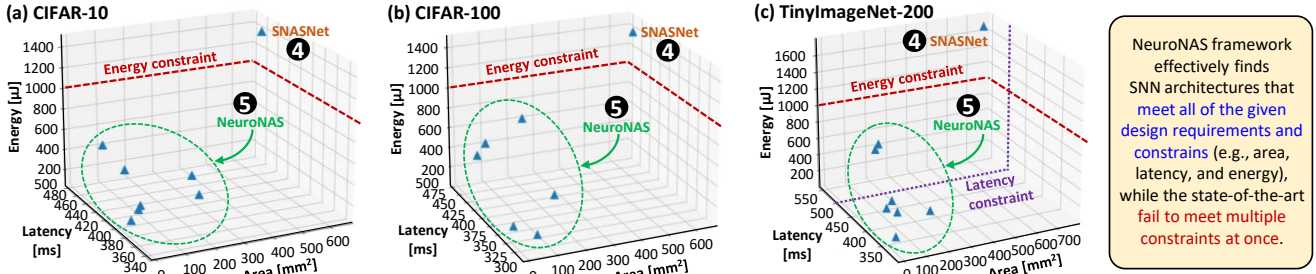


Fig. 12. Experimental results of the hardware area, processing latency, and energy consumption achieved by the SNASNet and our NeuroNAS across different precision levels (i.e., FxP16, FxP14, FxP12, FxP10, FxP8, FxP6, and FxP4) for (a) CIFAR-10, (b) CIFAR-100, and (c) TinyImageNet-200 workloads.

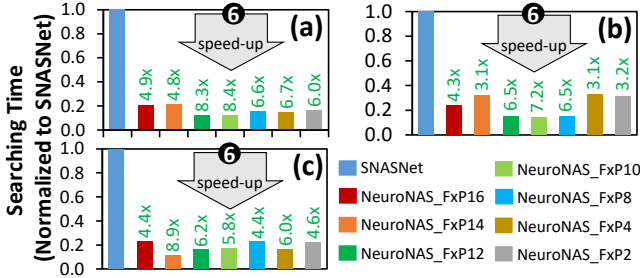


Fig. 13. Experimental results of the searching time achieved by the SNASNet and our NeuroNAS across different precision levels (i.e., FxP16, FxP14, FxP12, FxP10, FxP8, FxP6, and FxP4) for (a) CIFAR-10, (b) CIFAR-100, and (c) TinyImageNet-200 workloads.

for CIFAR-100 (67%-96% savings from SNASNet), and 25mm<sup>2</sup>-166mm<sup>2</sup> for TinyImageNet-200 (78%-96% savings from SNASNet) across different precision levels; see 5. These indicate that *NeuroNAS can ensure the generated network to meet the area constraint*, which also leads to smaller area costs compared to SNASNet. The reason is that, NeuroNAS includes the area requirement in its NAS process, hence making it possible to develop both networks and CIM hardware within a custom area budget.

**Latency:** SNASNet generates networks that have latency of 468ms for both CIFAR-10 and CIFAR-100, and 545ms for TinyImageNet-200, which does not meet the latency constraint; see 4. The reason is that, SNASNet does not consider the latency budget in its NAS process. Meanwhile, our NeuroNAS generates networks that have latency of 340ms-494ms for CIFAR-10, 315ms-494mm for CIFAR-100 and TinyImageNet-200 across different precisions; see 5. These show that *NeuroNAS can ensure the generated network to fulfill the latency constraint*, since it considers the latency information in its NAS process, hence making it possible to develop both networks and CIM hardware within a custom latency budget.

**Energy Consumption:** SNASNet generates networks that incur energy consumption about 1425μJ for both CIFAR-10 and CIFAR-100, and 1696μJ for TinyImageNet-200, hence they do not meet the energy budget; see 4. The reason is that, SNASNet does not consider the energy budget in its NAS process and focuses only on accuracy. Moreover, in each neural cell, there are multiple CONV

layers which cannot be mapped in the same CIM tile due to the mapping strategy, which forces the CIM processing to utilize more compute resources (e.g., CIM tiles), which in turn leading to higher energy consumption. Our NeuroNAS addresses these limitations by incorporating the energy budget in its NAS, hence avoiding the energy consumption to surpass the given constraint. Specifically, NeuroNAS generates networks that incur energy consumption of 127μJ-576μJ for CIFAR-10 (59%-91% savings from SNASNet), 110μJ-712μJ for CIFAR-100 (50%-92% savings from SNASNet), and 110μJ-644μJ for TinyImageNet-200 (74%-93% savings from SNASNet) across different precision levels; see 5.

### C. Searching Time Speed-Up

Fig. 13 presents the experimental results of the searching time. In general, our NeuroNAS offers significant speed-ups for the searching time as compared to the state-of-the-art. Specifically, NeuroNAS improves the searching time by 4.8x-8.4x for CIFAR-10, by 3.1x-7.2x for CIFAR-100, and by 4.4x-8.9x for TinyImageNet-200. The reason is that, our NeuroNAS employs a fewer SNN operations, minimizes redundant architecture candidates to evaluate, incorporates multiple constraints into the search process, hence leading to a smaller search space and a faster searching time as compared to the state-of-the-art.

In summary, *our NeuroNAS can quickly provide an SNN that fulfills the given memory, area, latency, and energy constraints*. For instance, NeuroNAS\_FxP8 maintains high accuracy comparable to the state-of-the-art, while achieving up to 92% area savings, 1.2x latency speed-ups, 84% energy savings, and 6.6x search time speed-ups.

## VI. CONCLUSION

We propose the NeuroNAS framework to find an SNN architecture that achieves high accuracy under multiple constraints. It is achieved by optimizing SNN operations, developing an efficient SNN using novel QaFE policy, and designing a hardware-aware search algorithm that includes the given constraints in its NAS. As a result, NeuroNAS maintains high accuracy comparable to state-of-the-art while improving other aspects to meet all constraints. For instance, NeuroNAS\_FxP8 achieves up to 92% area savings, 1.2x latency speed-ups, 84% energy savings, and 6.6x search time speed-ups across all datasets. In this manner, our NeuroNAS framework enables the efficient design automation for developing neuromorphic CIM systems for diverse application use-cases.

## REFERENCES

- [1] B. Na, J. Mok, S. Park, D. Lee, H. Choe, and S. Yoon, "Autosnn: Towards energy-efficient spiking neural networks," in *International Conference on Machine Learning (ICML)*, 2022, pp. 16253–16269.
- [2] Y. Kim, Y. Li, H. Park, Y. Venkatesha, and P. Panda, "Neural architecture search for spiking neural networks," in *European Conference on Computer Vision (ECCV)*. Springer, 2022, pp. 36–56.
- [3] R. V. W. Putra and M. Shafique, "Spikenas: A fast memory-aware neural architecture search framework for spiking neural network systems," *arXiv preprint arXiv:2402.11322*, 2024.
- [4] F. Akopyan, J. Sawada, A. Cassidy, R. Alvarez-Icaza, J. Arthur, P. Merolla, N. Imam, Y. Nakamura, P. Datta, G. Nam, B. Taba, M. Beakes, B. Brezzo, J. B. Kuang, R. Manohar, W. P. Risk, B. Jackson, and D. S. Modha, "Truenorth: Design and tool flow of a 65 mw 1 million neuron programmable neurosynaptic chip," *IEEE Transactions on Computer-Aided Design of Integrated Circuits and Systems (TCAD)*, vol. 34, no. 10, Oct 2015.
- [5] M. Davies, N. Srinivasa, T. Lin, G. Chinya, Y. Cao, S. H. Choday, G. Dimou, P. Joshi, N. Imam, S. Jain, Y. Liao, C. Lin, A. Lines, R. Liu, D. Mathaikutty, S. McCoy, A. Paul, J. Tse, G. Venkataramanan, Y. Weng, A. Wild, Y. Yang, and H. Wang, "Loihi: A neuromorphic manycore processor with on-chip learning," *IEEE Micro*, vol. 38, no. 1, pp. 82–99, Jan 2018.
- [6] A. Basu, L. Deng, C. Frenkel, and X. Zhang, "Spiking neural network integrated circuits: A review of trends and future directions," in *IEEE Custom Integrated Circuits Conference (CICC)*, 2022, pp. 1–8.
- [7] N. Rathi, P. Panda, and K. Roy, "Stdp-based pruning of connections and weight quantization in spiking neural networks for energy-efficient recognition," *IEEE Transactions on Computer-Aided Design of Integrated Circuits and Systems (TCAD)*, vol. 38, no. 4, pp. 668–677, 2019.
- [8] R. V. W. Putra and M. Shafique, "Fspinn: An optimization framework for memory-efficient and energy-efficient spiking neural networks," *IEEE Transactions on Computer-Aided Design of Integrated Circuits and Systems (TCAD)*, vol. 39, no. 11, pp. 3601–3613, 2020.
- [9] L. Cordone, B. Miramond, and P. Thierion, "Object detection with spiking neural networks on automotive event data," in *International Joint Conference on Neural Networks (IJCNN)*, July 2022, pp. 1–8.
- [10] R. V. W. Putra, A. Marchisio, and M. Shafique, "Snn4agents: A framework for developing energy-efficient embodied spiking neural networks for autonomous agents," *Frontiers in Robotics and AI (FROBT)*, vol. 11, 2024.
- [11] M. F. Minhas, R. V. W. Putra, F. Awwad, O. Hasan, and M. Shafique, "Continual learning with neuromorphic computing: Theories, methods, and applications," *arXiv preprint arXiv:2410.09218*, 2024.
- [12] J. M. Allred and K. Roy, "Controlled forgetting: Targeted stimulation and dopaminergic plasticity modulation for unsupervised lifelong learning in spiking neural networks," *Frontiers in Neuroscience (FNINS)*, vol. 14, p. 7, 2020.
- [13] R. V. W. Putra and M. Shafique, "Spikedyn: A framework for energy-efficient spiking neural networks with continual and unsupervised learning capabilities in dynamic environments," in *58th ACM/IEEE Design Automation Conference (DAC)*, 2021, pp. 1057–1062.
- [14] —, "Ipspikecon: Enabling low-precision spiking neural network processing for efficient unsupervised continual learning on autonomous agents," in *International Joint Conference on Neural Networks (IJCNN)*, 2022, pp. 1–8.
- [15] C. Bartolozzi, G. Indiveri, and E. Donati, "Embodied neuromorphic intelligence," *Nature communications*, vol. 13, no. 1, p. 1024, 2022.
- [16] Y. Luo, Q. Fu, J. Xie, Y. Qin, G. Wu, J. Liu, F. Jiang, Y. Cao, and X. Ding, "Eeg-based emotion classification using spiking neural networks," *IEEE Access*, vol. 8, pp. 46 007–46 016, 2020.
- [17] A. Ankit, A. Sengupta, P. Panda, and K. Roy, "Resparc: A reconfigurable and energy-efficient architecture with memristive crossbars for deep spiking neural networks," in *54th Annual Design Automation Conference (DAC)*, 2017, pp. 1–6.
- [18] A. Moitra, A. Bhattacharjee, R. Kuang, G. Krishnan, Y. Cao, and P. Panda, "Spikesim: An end-to-end compute-in-memory hardware evaluation tool for benchmarking spiking neural networks," *IEEE Transactions on Computer-Aided Design of Integrated Circuits and Systems*, vol. 42, no. 11, pp. 3815–3828, 2023.
- [19] A. Roy, S. Venkataramani, N. Gala, S. Sen, K. Veezhinathan, and A. Raghunathan, "A programmable event-driven architecture for evaluating spiking neural networks," in *IEEE/ACM International Symposium on Low Power Electronics and Design (ISLPED)*, July 2017, pp. 1–6.
- [20] S. Sen, S. Venkataramani, and A. Raghunathan, "Approximate computing for spiking neural networks," in *Design, Automation Test in Europe Conference and Exhibition (DATE)*, 2017, March 2017, pp. 193–198.
- [21] S. Krithivasan, S. Sen, S. Venkataramani, and A. Raghunathan, "Dynamic spike bundling for energy-efficient spiking neural networks," in *IEEE/ACM International Symposium on Low Power Electronics and Design (ISLPED)*, July 2019, pp. 1–6.
- [22] Y. Wu, L. Deng, G. Li, J. Zhu, Y. Xie, and L. Shi, "Direct training for spiking neural networks: Faster, larger, better," in *AAAI Conference on Artificial Intelligence (AAAI)*, vol. 33, no. 01, 2019, pp. 1311–1318.
- [23] W. Fang, Z. Yu, Y. Chen, T. Masquelier, T. Huang, and Y. Tian, "Incorporating learnable membrane time constant to enhance learning of spiking neural networks," in *IEEE/CVF International Conference on Computer Vision (ICCV)*, 2021, pp. 2661–2671.
- [24] C. Lee, S. S. Sarwar, P. Panda, G. Srinivasan, and K. Roy, "Enabling spike-based backpropagation for training deep neural network architectures," *Frontiers in Neuroscience (FNINS)*, p. 119, 2020.
- [25] H. Zheng, Y. Wu, L. Deng, Y. Hu, and G. Li, "Going deeper with directly-trained larger spiking neural networks," in *AAAI Conference on Artificial Intelligence (AAAI)*, vol. 35, no. 12, 2021, pp. 11 062–11 070.
- [26] Q. Liu, J. Yan, M. Zhang, G. Pan, and H. Li, "Lite-snn: Designing lightweight and efficient spiking neural network through spatial-temporal compressive network search and joint optimization," *arXiv preprint arXiv:2401.14652*, 2024.
- [27] J. Yan, Q. Liu, M. Zhang, L. Feng, D. Ma, H. Li, and G. Pan, "Efficient spiking neural network design via neural architecture search," *Neural Networks*, p. 106172, 2024.
- [28] W. Pan, F. Zhao, G. Shen, B. Han, and Y. Zeng, "Multi-scale evolutionary neural architecture search for deep spiking neural networks," *arXiv preprint arXiv:2304.10749*, 2023.
- [29] K. Che, Z. Zhou, Z. Ma, W. Fang, Y. Chen, S. Shen, L. Yuan, and Y. Tian, "Auto-spikformer: Spikformer architecture search," *arXiv preprint arXiv:2306.00807*, 2023.
- [30] Z. Wang, Q. Zhao, J. Cui, X. Liu, and D. Xu, "Autost: Training-free neural architecture search for spiking transformers," in *IEEE International Conference on Acoustics, Speech and Signal Processing (ICASSP)*. IEEE, 2024, pp. 3455–3459.
- [31] J. Mellor, J. Turner, A. Storkey, and E. J. Crowley, "Neural architecture search without training," in *International Conference on Machine Learning (ICML)*, 2021, pp. 7588–7598.
- [32] X. Dong and Y. Yang, "Nas-bench-201: Extending the scope of reproducible neural architecture search," in *International Conference on Learning Representations (ICLR)*, 2020.
- [33] H. Benmeziane, A. Z. Ounnoughene, I. Hamzaoui, and Y. Bouhadjar, "Skip connections in spiking neural networks: An analysis of their effect on network training," in *IPDPSW Workshop Scalable Deep Learning over Parallel And Distributed Infrastructures (ScadL)*, 2023.
- [34] J. D. Nunes, M. Carvalho, D. Carneiro, and J. S. Cardoso, "Spiking neural networks: A survey," *IEEE Access*, vol. 10, 2022.
- [35] R. V. W. Putra, M. A. Hanif, and M. Shafique, "Sparkxd: A framework for resilient and energy-efficient spiking neural network inference using approximate dram," in *58th ACM/IEEE Design Automation Conference (DAC)*, 2021, pp. 379–384.
- [36] —, "Respawn: Energy-efficient fault-tolerance for spiking neural networks considering unreliable memories," in *2021 IEEE/ACM International Conference On Computer Aided Design (ICCAD)*. IEEE, 2021, pp. 1–9.
- [37] Y. Li, A. Moitra, T. Geller, and P. Panda, "Input-aware dynamic timestep spiking neural networks for efficient in-memory computing," in *2023 60th ACM/IEEE Design Automation Conference (DAC)*, 2023, pp. 1–6.
- [38] W. Fang, Y. Chen, J. Ding, Z. Yu, T. Masquelier, D. Chen, L. Huang, H. Zhou, G. Li, and Y. Tian, "Spikingjelly: An open-source machine learning infrastructure platform for spike-based intelligence," *Science Advances*, vol. 9, no. 40, 2023.
- [39] Y. Wu, L. Deng, G. Li, J. Zhu, and L. Shi, "Spatio-temporal backpropagation for training high-performance spiking neural networks," *Frontiers in Neuroscience (FNINS)*, vol. 12, p. 331, 2018.
- [40] E. O. Neftci, H. Mostafa, and F. Zenke, "Surrogate gradient learning in spiking neural networks: Bringing the power of gradient-based optimization to spiking neural networks," *IEEE Signal Processing Magazine (MSP)*, vol. 36, no. 6, pp. 51–63, 2019.
- [41] B. Hajri, H. Aziza, M. M. Mansour, and A. Chehab, "Rram device models: A comparative analysis with experimental validation," *IEEE Access*, vol. 7, pp. 168 963–168 980, 2019.